

Resonant production of diquarks at high energy pp, ep and e^+e^- colliders

O. Cakir and M. Sahin

Ankara University, Faculty of Sciences, Department of Physics, 06100, Tandoğan, Ankara, Turkey

Resonant productions of the first generation scalar and vector diquarks at high energy hadron-hadron (pp), lepton-hadron (ep) and lepton-lepton (e^+e^-) colliders are investigated. Taking into account the hadronic component of the photon, diquarks can be produced resonantly in the lepton-hadron and lepton-lepton collisions. Production rates, decay widths and signatures of diquarks are discussed using the general, $SU(3)_C \times SU(2)_W \times U(1)_Y$ invariant, effective Lagrangian. The corresponding dijet backgrounds are examined in the interested invariant mass regions. The attainable mass limits and couplings are obtained for the diquarks that can be produced in hadron collisions and in resolved photon processes. It is shown that hadron collider with center of mass energy $\sqrt{s} = 14$ TeV will be able to discover scalar and vector diquarks with masses up to $m_{D_Q} = 9$ TeV for quark-diquark-quark coupling $\alpha_{D_Q} = 0.1$. Relatively, lighter diquarks can be probed at ep and e^+e^- collisions in more clear environment.

I. INTRODUCTION

Diquarks can occur in many scenarios which involve new physics beyond the standard model (SM), e.g., composite models [1] and superstring-inspired E_6 models [2]. These particles can transform as anti-triplet (3) or sextet (6) under $SU(3)$. Diquarks carry baryon number $B_j = 2=3$ and couple to a pair of quarks. They have integer spin (scalar or vector) and have electric charges $Q_j = 1=3; 2=3$ or $4=3$.

The Collider Detector at Fermilab (CDF) has set limits on the masses of a class of scalar diquarks decaying to dijets with the exclusion of mass range $290 < m_{D_Q} < 420$ GeV [3], which are expected to be approximately valid for other scalar diquarks. There are also indirect bounds imposed on couplings from electroweak precision data [4] from LEP e^+e^- collider where these bounds allow diquark-quark couplings up to a value $\alpha_{D_Q} = 0.1$.

Three types of the colliders related to the energy frontiers in particle physics research seem to be promising in the next decade. Namely, they are Large Hadron Collider (LHC) with the center of mass energy $\sqrt{s} = 14$ TeV and luminosity $L = 10^{34} - 10^{35} \text{ cm}^{-2} \text{ s}^{-1}$, International Linear Collider (ILC) with $\sqrt{s} = 0.5$ TeV and $L = 10^{34} - 10^{35} \text{ cm}^{-2} \text{ s}^{-1}$; Compact Linear Collider (CLIC) with $\sqrt{s} = 3$ TeV and $L = 10^{34} - 10^{35} \text{ cm}^{-2} \text{ s}^{-1}$ in the most preferable design, and the linac-ring type ep colliders, when the linear collider is constructed near the proton ring, i.e., ILC - LHC based ep collider with $\sqrt{s} = 2.64$ TeV and CLIC - LHC based ep collider with $\sqrt{s} = 3.74$ TeV or $\sqrt{s} = 6.48$ TeV, having a luminosity $L = 10^{31} - 10^{32} \text{ cm}^{-2} \text{ s}^{-1}$. Even though the last one has a lower luminosity it can provide better conditions for investigations of a lot of phenomena comparing to ILC due to the essentially higher center of mass energy and LHC due to more clear environment. The high energy linear e^+e^- colliders have been proposed as the instruments that can perform measurements that would complement those performed at the LHC. The

TABLE I: The main parameters of the future ep and e^+e^- colliders, L^{int} denotes the integrated luminosity for one working year.

| ep Colliders | | E_e (TeV) | E_p (TeV) | $\sqrt{s_{ep}}$ (TeV) | L_{ep}^{int} (10^2 pb^{-1}) |
|--------------------|-----|-----------------|-------------|---------------------------|--|
| ILC | LHC | 0.25 | 7 | 2.64 | 1 10 |
| CLIC | LHC | 0.5 | 7 | 3.74 | 1 10 |
| CLIC | LHC | 1.5 | 7 | 6.48 | 1 10 |
| e^+e^- Colliders | | E_{e^+} (TeV) | E_e (TeV) | $\sqrt{s_{e^+e^-}}$ (TeV) | $L_{e^+e^-}^{\text{int}}$ (10^5 pb^{-1}) |
| ILC | | 0.25 | 0.25 | 0.5 | 1 10 |
| CLIC | | 0.5 | 0.5 | 1.0 | 1 10 |
| CLIC | | 1.5 | 1.5 | 3.0 | 1 10 |

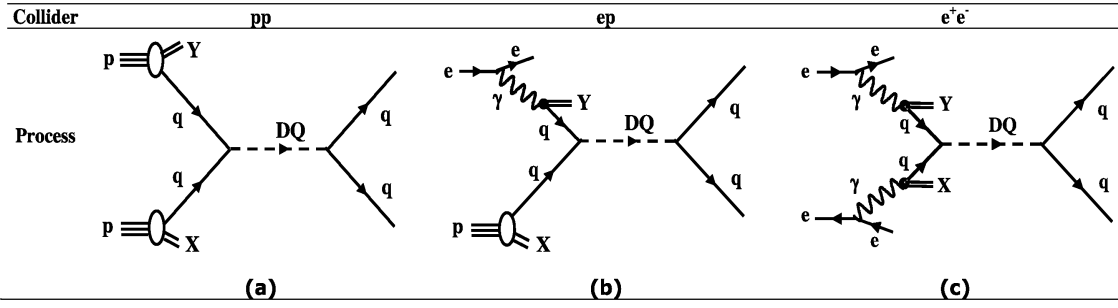


FIG. 1: Schematic presentation of resonant production of scalar or vector diquarks at three types of colliders: a) pp collisions, b) ep collisions with one resolved photon process and c) e^+e^- collisions with two resolved photon process.

diquarks are expected to be easily observable at LHC through their resonant production and subsequent decay to two jets. If relatively light diquarks are observed at LHC they are expected to be in the reach of the future linear e^+e^- and linac-ring type ep colliders. The main parameters of future ep and e^+e^- colliders are given in Table I.

The production and possibility of detection of diquarks have been analysed for e^+e^- [5], $p\bar{p}$ [6, 7] and pp [8, 9] colliders. The single and pair production of scalar diquarks in ep collisions have been analysed in [10] without taking into account hadronic structure of the photon. Although the photon is the gauge particle of the electromagnetic interactions and thus pointlike, it is known to behave like a hadron if it interacts with other hadrons. This can be described by the QCD-corrected quark parton model if the photon is probed at a large momentum scale. The importance of resolved photon contributions has been demonstrated by the DELPHI [11] and OPAL [12] Collaborations in obtaining interesting limits on leptoquark properties from e^- production of leptoquarks [13]. The relevance of the photon substructure increases with increasing center of mass energy and becomes therefore important for forthcoming ep and e^+e^- colliders.

In this work, we investigate the potentials of high energy pp, ep and e^+e^- colliders to search for scalar and vector diquarks via their resonant production subprocesses

$$q\bar{q} \rightarrow DQ \rightarrow 2j \quad (1)$$

$$q\bar{q} \rightarrow DQ \rightarrow 2j \quad (2)$$

$$q\bar{q} \rightarrow DQ \rightarrow 2j \quad (3)$$

where q is the quark from resolved photon. The second process can also be considered as a contribution to the single diquark production at ep colliders. We analyze the relevant background processes in the cases of three-type of collisions. Schematic presentation of resonant production of diquarks at three types of colliders is shown in Fig. 1 (a-c).

II. INTERACTION LAGRANGIAN

A model independent, baryon number conserving, most general $SU(3)_C \times SU(2)_W \times U(1)_Y$ invariant effective lagrangian for scalar and vector diquarks has the form [8, 9]

$$\begin{aligned} L_{\mathcal{B} j=0} = & f_{1L} \bar{q}_L^C q_L D Q_1^C + (f_{1R} \bar{d}_R^C d_R + f_{1R}^0 \bar{u}_R^C u_R) D Q_1^C \\ & + f_{1R} \bar{u}_R^C d_R \mathcal{D} Q_1^C + f_{3L} \bar{q}_L^C q_L D Q_3^C \\ & + f_2 \bar{q}_L^C i_2 u_R D Q_2^C + f_2^0 \bar{q}_L^C i_2 d_R \mathcal{D} Q_2^C + H.c. \end{aligned} \quad (4)$$

$$\begin{aligned} L_{\mathcal{B} j=2=3} = & (g_{1L} \bar{q}_L^C i_2 q_L + g_{1R} \bar{u}_R^C d_R) D Q_1^C + g_{1R} \bar{d}_R^C d_R \mathcal{D} Q_1^C \\ & + g_{1R}^0 \bar{u}_R^C u_R \mathcal{D} Q_1^C + g_{3L} \bar{q}_L^C i_2 q_L D Q_3^C \\ & + g_2 \bar{q}_L^C d_R D Q_2^C + g_2^0 \bar{q}_L^C u_R \mathcal{D} Q_2^C + H.c. \end{aligned} \quad (5)$$

where the $\mathcal{B} j=0$ diquarks are familiar fields, as they resemble the electroweak gauge vectors, and the neutral and charged Higgs scalars. Here, we consider only the $\mathcal{B} j=2=3$ diquarks. In Eq. (4) and (5), $q_L = (u_L; d_L)$ denotes the

TABLE II: Quantum numbers of the first generation, color 3 diquarks described by the effective lagrangian in the text according to $SU(3)_C \times SU(2)_W \times U(1)_Y$ invariance where the hypercharge $Y = 2(Q - I_3)$.

| | $SU(3)_C$ | $SU(2)_W$ | $U(1)_Y$ | Q | Couplings |
|-----------------|-----------|-----------|----------|---|--|
| Scalar Diquarks | | | | | |
| $D_Q 1$ | 3^2 | 1 | $2/3$ | $1/3$ | $u_L d_L (g_{1L}) ; u_R d_R (g_{1R})$ |
| $\bar{D} Q_1^0$ | 3^2 | 1 | $-4/3$ | $2/3$ | $d_R d_R (g_{1R})$ |
| $\bar{D} Q_1^0$ | 3^2 | 1 | $8/3$ | 0 | $u_R u_R (g_{1R}^0)$ |
| | | | | $4=3$ | $u_L u_L (\frac{p}{2g_{3L}})$ |
| $D_Q 3$ | 3^2 | 3 | $2/3$ | $\bar{B} \quad \begin{smallmatrix} 1=3 \\ \bar{A} \end{smallmatrix} \quad \begin{smallmatrix} B \\ \bar{A} \end{smallmatrix}$ | $u_L d_L (\frac{p}{2g_{3L}}) \quad \begin{smallmatrix} C \\ \bar{A} \end{smallmatrix}$ |
| | | | | $2=3$ | $d_L d_L (\frac{p}{2g_{3L}})$ |
| Vector Diquarks | | | | | |
| $D_Q 2$ | 3^2 | 2 | $-1/3$ | $1=3$ | $d_R u_L (g_2)$ |
| | | | | $2=3$ | $d_R d_L (g_2) !$ |
| $\bar{D} Q_2^0$ | 3^2 | 2 | $5/3$ | $4=3$ | $u_R u_L (g_2)$ |
| | | | | $1=3$ | $u_R d_L (g_2)$ |

left handed quark spinor and $q^c = C q^T$ ($q^c = q^T C^{-1}$) is the charge conjugated quark field. Following [8, 9], the possible scalar and vector diquarks are $SU(3)_C$ anti-triplets and sextets. For the sake of simplicity, color and generation indices are omitted in (4) and (5). Scalar diquarks $D_Q 1$, $\bar{D} Q_1^0$, $\bar{D} Q_1^0$ are $SU(2)_W$ singlets and $D_Q 3$ is $SU(2)_W$ triplet. Vector diquarks $D_Q 2$ and $\bar{D} Q_2^0$ are $SU(2)_W$ doublets. At this stage, we assume that each SM generation has its own diquarks and couplings in order to avoid flavour changing neutral currents (FCNC). Furthermore, the members of a given multiplet are assumed to be the mass degenerated. A general classification of the first generation, color anti-triplet (3) diquarks is shown in Table II.

For the present analysis, we consider the color 3 scalar $D_Q 1$ or $D_Q 3^0$ diquarks coupled to ud pairs, $\bar{D} Q_1^0$ or $D_Q 3^2$ diquarks coupled to dd pair and $\bar{D} Q_1^0$ or $D_Q 3^2$ diquarks coupled to uu pair. The vector diquarks $D_Q 2^1$ and $\bar{D} Q_2^2$ of type ud , $D_Q 2^2$ of type dd and $\bar{D} Q_2^1$ of type uu are considered. The interaction between the diquark and quark pair is described by the effective lagrangian (5) with different couplings.

III. DECAY WIDTHS

For the decay width calculation, we take the coupling as $g_{D_Q}^2 = g_L^2 + g_R^2$ for each diquark type. For numerical results, we will use the definition $g_{D_Q}^2 = 4 g_{D_Q}$ when only one type of coupling assumed to be nonzero. Diquarks decay into quark pairs, and the decay width Γ_{D_Q} derived from the same lagrangian is

$$\frac{\Gamma_{D_Q}}{S} = \frac{F_S g_{D_Q}^2 m_{D_Q}}{16} \cdot 25 \text{ GeV} \left(\frac{F_S m_{D_Q}}{1 \text{ TeV}} \right) \quad \text{for } D_Q = 0:1 \quad (6)$$

$$\frac{\Gamma_{D_Q}}{V} = \frac{F_S g_{D_Q}^2 m_{D_Q}}{24} \cdot 17 \text{ GeV} \left(\frac{F_S m_{D_Q}}{1 \text{ TeV}} \right) \quad \text{for } D_Q = 0:1 \quad (7)$$

where F_S contains the color factor for a representation including the statistical factors associated with the presence of identical fermions in the final state, and m_{D_Q} is the mass of scalar (S) or vector (V) diquark.

IV. SIGNAL AND BACKGROUND

The signal for diquark production would clearly manifest itself in two jets cross sections. The differential cross section for any type of scalar and vector diquark resonant production can be written as follows

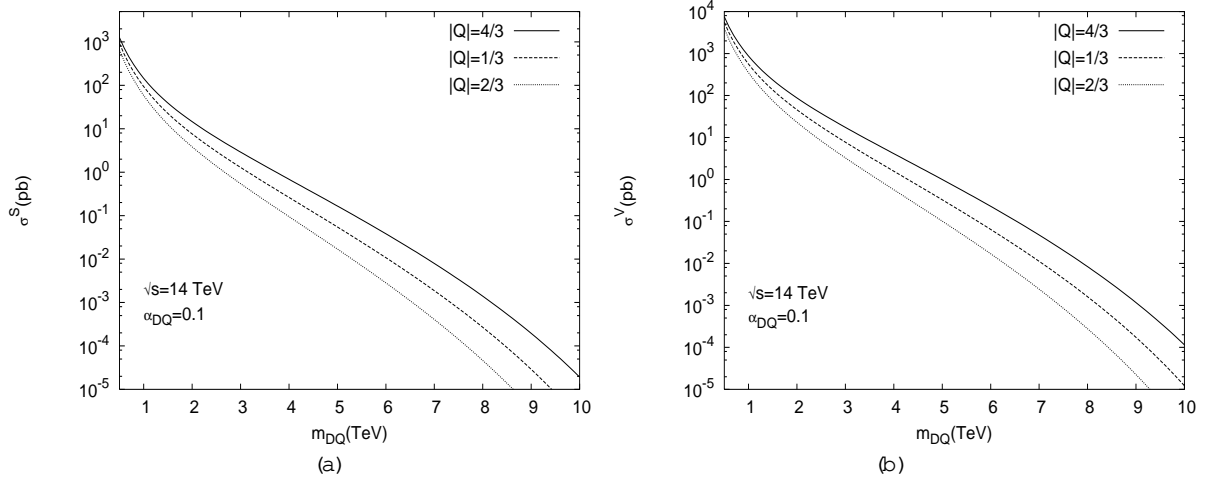


FIG. 2: Total cross sections in pp collisions for a) scalar and b) vector diquarks for diquark charges, with coupling strength $\alpha_{DQ} = 0.1$, depending on their masses.

$$\frac{d^S}{dt} (q_i q_j \rightarrow DQ \rightarrow q_i q_j) = \frac{F_S g_{DQ}^4}{64 [(\frac{s}{m_{DQ}})^2 + (\frac{m_{DQ}}{s_{DQ}})^2]} \quad (8)$$

$$\frac{d^V}{dt} (q_i q_j \rightarrow DQ \rightarrow q_i q_j) = \frac{F_S g_{DQ}^4}{16 [(\frac{s}{m_{DQ}})^2 + (\frac{m_{DQ}}{s_{DQ}})^2]} \quad (9)$$

In the narrow width approximation ($m_{DQ} = m_{DQ} < 0.1$), the cross section of the s channel diquark production can be obtained as

$$\hat{\sigma}_R^S (b) \sim \frac{F_S g_{DQ}^4 b}{64 m_{DQ} s_{DQ}} (b - m_{DQ}^2) \quad (10)$$

$$\hat{\sigma}_R^V (b) \sim \frac{F_S g_{DQ}^4 b}{16 m_{DQ} s_{DQ}} (b - m_{DQ}^2) \quad (11)$$

where b is the Mandelstam variable corresponding to the square of center-of-mass energy for the subprocess.

A. pp Collider

The total cross section for the resonance production of scalar diquarks at pp collider is given by

$$= \int_{m_{DQ}^2/s}^{Z_1} \frac{dx}{x} f_{q=p}(x; Q_p^2) f_{q^0=p}(m_{DQ}^2 = xs; Q_p^2) b(b) \quad (12)$$

where $f_{q=p}(x; Q_p^2)$ and $f_{q^0=p}(x; Q_p^2)$ correspond to the quark distribution functions from the proton and we have used CTEQ5L [14] parametrization with $Q_p^2 = b$. As a consequence of this energy scan there will be quarks whose energies are adequate for the resonance production of diquarks. The cross section is plotted against the diquark mass in Fig. 2 (a-b) for LHC energy ($\sqrt{s} = 14$ TeV) and coupling $\alpha_{DQ} = 0.1$. From these figures we find that diquarks with charge $|Q|=4/3$ have the largest cross sections when compared to the other types.

The scalar and vector diquarks will decay via $DQ \rightarrow q_i q_j$. Therefore, the relevant signal will be a pair of hard jets in the final state. At the LHC energy, major QCD background processes contributing to two-jet (2j) final states and their integrated cross sections are given in Table III.

TABLE III: The cross sections (in pb) for QCD backgrounds contributing to two jets final states at parton level generated by CompHEP with various p_T cuts.

| Process | $p_T > 0.1$ TeV | $p_T > 0.5$ TeV | $p_T > 1$ TeV | $p_T > 2$ TeV |
|-----------------------------------|------------------|------------------|---------------------|---------------------|
| gg + gg | $6.3 \cdot 10^5$ | $2.0 \cdot 10^2$ | $2.3 \cdot 10^0$ | $5.7 \cdot 10^{-3}$ |
| qg + qg | $6.4 \cdot 10^5$ | $4.8 \cdot 10^2$ | $1.0 \cdot 10^1$ | $5.7 \cdot 10^{-2}$ |
| qq ⁰ + qq ⁰ | $1.0 \cdot 10^5$ | $1.8 \cdot 10^2$ | $6.7 \cdot 10^0$ | $8.8 \cdot 10^{-2}$ |
| gg + q <bar>q</bar> | $2.4 \cdot 10^4$ | $9.8 \cdot 10^0$ | $1.0 \cdot 10^{-1}$ | $2.9 \cdot 10^{-4}$ |
| q <bar>q</bar> + q <bar>q</bar> | $1.6 \cdot 10^3$ | $2.8 \cdot 10^0$ | $1.3 \cdot 10^{-1}$ | $1.1 \cdot 10^{-3}$ |
| q <bar>q</bar> + gg | $1.5 \cdot 10^3$ | $2.5 \cdot 10^0$ | $6.7 \cdot 10^{-2}$ | $8.5 \cdot 10^{-4}$ |
| Total | $1.4 \cdot 10^6$ | $8.8 \cdot 10^2$ | $1.9 \cdot 10^1$ | $1.5 \cdot 10^{-1}$ |

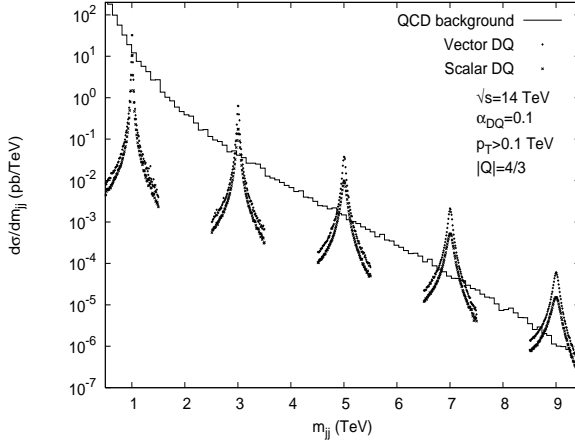


FIG. 3: Dijet invariant mass distributions for $pp + 2jX$: Resonance peaks are shown for scalar and vector diquark masses 1, 3, 5, 7, and 9 TeV for comparison with smooth QCD backgrounds.

The values in Table III have been generated by CompHEP program [15] at parton level with various p_T cuts on the jets. It is clear that higher p_T cuts reduce the background cross sections significantly. These p_T cuts can be translated into the rapidity cuts according to the relation between the p_T of a jet and the rapidity with $p_T = m_{jj} = 2 \cosh y$. Standard kinematic relations for the invariant mass m_{jj} and p_T distributions of two-jet final states can be found in [8, 9]. Figure 3 shows the dijet invariant mass distribution for the process $pp + 2jX$ including the signal and the QCD backgrounds at the LHC. For comparison signal peaks for scalar and vector diquark masses $m_{DQ} = 1; 3; 5; 7; 9$ TeV and $\alpha_{DQ} = 0.1$ are shown on the smooth background distribution.

In order to obtain the observability of diquarks at LHC we have calculated signal (S) and background (B) event estimations for an integrated luminosity of 10^5 pb⁻¹. The signal generated by a diquark of mass m_{DQ} and decay rate α_{DQ} is calculated integrating the differential cross section in the two-jet invariant mass interval $m_{DQ} - \Delta_{DQ} < m_{jj} < m_{DQ} + \Delta_{DQ}$ which embraces approximately 95% of the events around the resonance. For a realistic analysis of the background events we take into account the finite energy resolution of the LHC ATLAS hadronic calorimeter [16] as $E = E_{\perp} = 0.5 = E_{\parallel} + 0.03$ for jets with $|y| < 3$. The corresponding two-jet invariant mass resolution is given approximately by $m_{jj} = 0.5 \sqrt{m_{jj}^2 + 0.02m_{jj}}$. The background is calculated by integrating the cross sections in the range $m_{DQ} - \Delta_{DQ} < m_{jj} < m_{DQ} + \Delta_{DQ}$ with $\Delta_{DQ} = \max(\Delta_{DQ}; m_{jj})$. The significance of signal over background is defined as $S = \sqrt{B}$. In Fig. 4 we present $S = \sqrt{B}$ as a function of the diquark mass for the scalar and vector diquarks with charges $Q_j = 4/3$ and $2/3$:

If we take at least 25 signal events and $S = \sqrt{B} = 5$ as discovery criteria, scalar (vector) diquarks with charge $Q_j = 2/3$ can be observed up to 7.5 (8.5) TeV. For the diquarks with charge $Q_j = 4/3$ it is possible to cover mass ranges up to 9.5 (10) TeV at the LHC with $L_{\text{int}} = 10^5$ pb⁻¹. For this luminosity, 10^7 scalar diquark events/year and 10^8 vector diquark events/year are expected for $m_{DQ} = 1$ TeV. Our results show that even for much lower coupling constants as 10^{-3} , diquarks should be seen at the LHC.

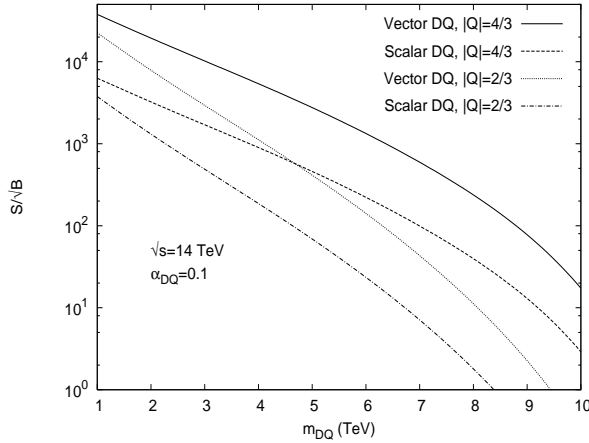


FIG . 4: The signal signi cance $S = \frac{P_B}{S_B}$ for diquarks as a function of diquark mass m_{DQ} at the LHC .

B . ep collider

In order to calculate the total cross section for diquark production due to resolved photon process at ep colliders, we use the formula

$$= \frac{Z_1}{m_{DQ}^2 = s} \frac{dx}{x} \frac{Z_1}{x} \frac{dy}{y} f_{=e}(y) f_{q^0}(x=y; Q^2) f_{q=p}(m_{DQ}^2 = xs; Q_p^2) b(b) \quad (13)$$

where $f_{=e}(y)$ [18] and $f_{q^0}(x=y; Q^2)$ [17] corresponds to the photon energy spectrum and the probability density of finding a quark ($q0$) carrying a fraction $x=y$ of the energy of the electrons in the initial beam s , respectively. In (13) the integrals over the momentum fractions x and y are the mathematical representation of an energy scan performed by the partons coming from photons and protons. We use the photon spectrum $f_{=e}(y)$ resulting from bremsstrahlung [18] with the electron beam energy E_e

$$f_{=e}(y) = \frac{1 + (1-y)^2}{2y} \ln \frac{4E_e^2(1-y)^2}{m_e^2 y^2} + 2m_e^2 y \frac{1}{4E_e^2(1-y)} \frac{1}{m_e^2 y^2} \quad : \quad (14)$$

We present the cross sections for scalar diquarks against their masses for coupling $\alpha_{DQ} = 0.1$ and charges $Q_j = 4/3; 1=3$ and $2=3$ using the bremsstrahlung process in Fig. 5 at CLIC LHC based ep colliders with $\frac{P}{\sqrt{s_{ep}}} = 6.48$ TeV .

In order to see the potentials of possible options of ep colliders with different center of mass energies, we plot diquark production cross sections depending on the $\frac{P}{\sqrt{s_{ep}}}$. As seen from the Fig. 6 vector diquarks have larger cross sections than the scalar for the considered center of mass energy region. In principle, the vector and scalar type diquarks can be easily distinguished by the angular distribution of produced jets, the electric charge of diquarks can be determined by the interactions with photon.

In the resonant production mechanism of diquarks with resolved photon process in collision $ep ! DQ + X ! 2j + X$, most of the particles in the final state are expected to be lost in the beam pipe, the two exceptions being the quarks resulting from diquark decay. As a result, the relevant signal is a p_T balanced coplanar pair of jets and it will contain two hard jets in the final state. All the relevant interactions with the diquarks are implemented into the CompHEP [15] program . The decay width of diquarks and the cross sections for signal and background processes are calculated with this program .

In order to study contributing backgrounds we need to take into account all the diagrams contributing to two-jet final states. The process $ep ! 2j + X$ has potentially large QCD background. At the ep colliders, major processes contributing to two-jets (2j) final states and their integrated cross sections are given in Table IV .

The values in Table IV have been generated by CompHEP at parton level for transverse momentum cut of the jets $p_T > 100$ GeV . Fig. 7 shows jet-jet invariant mass distribution for the process $ep ! 2jX$ at CLIC LHC based ep collider with $\frac{P}{\sqrt{s_{ep}}} = 6.48$ TeV .

In our analysis, we determine the expected significance of the signal over background for collider parameters given in Table I for ep colliders. It is convenient to collect the data in two-jet invariant mass bins since the signal is

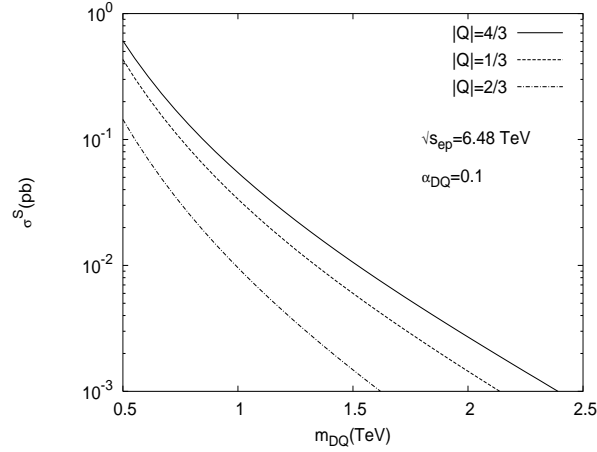


FIG. 5: The total cross sections for the process $e p \rightarrow D Q + X \rightarrow 2j + X$ at $\sqrt{s_{ep}} = 6.48$ TeV depending on the mass of scalar diquarks.

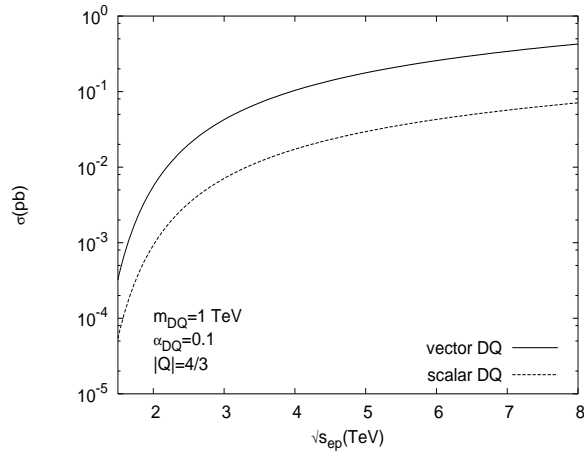


FIG. 6: The production cross sections $(e p \rightarrow D Q + X \rightarrow 2j + X)$ for scalar and vector diquarks with charge $|Q|=4/3$ and coupling $\alpha_{DQ} = 0.1$ depending the center of mass energy of the $e p$ colliders.

concentrated in a small region of the invariant mass spectrum. Therefore, we introduced the cut $|m_{jj} - m_{DQ}| < 25$ GeV which is efficient only for diquark masses between 0.5 and 1 TeV. For heavier diquarks rather broad resonances are expected and the cut $|m_{jj} - m_{DQ}| < 50$ GeV becomes suitable for $1 \text{ TeV} < m_{DQ} < 2.5 \text{ TeV}$. This range of the invariant mass will embrace approximately 95% of the signal events around the diquark resonance. For a realistic analysis we have estimated background events for $e p$ colliders with the integrated luminosity of 10^3 pb^{-1} taking into account the energy resolution of the hadronic calorimeter. The statistical significance $S = \sqrt{B}$ of diquark signal over background are shown in Fig. 8 for ILC-LHC and CLIC-LHC based $e p$ colliders. From Fig. 8, we find that scalar (vector) diquarks can be seen up to 1 (1.6) TeV at the $e p$ collider with $\sqrt{s} = 6.48$ TeV. A slightly lower limit can be obtained for the other $e p$ options.

If we take into account the integrated luminosity $L = 10^3 \text{ pb}^{-1}$ for the CLIC-LHC based $e p$ collider with $\sqrt{s} = 6.48$ TeV, 44 scalar diquark events and 264 vector diquark events/year are expected for $m_{DQ} = 1 \text{ TeV}$ and $\alpha_{DQ} = 0.1$.

TABLE IV : The major processes contributing to two jet (jj) final states with a cut $p_T > 100$ GeV at the ep collisions with different center of mass energy $\sqrt{s_{ep}}$.

| Collider | ILC | LHC | CLIC | LHC |
|-----------------------|-------|--------|-------|--------|
| $\sqrt{s_{ep}}$ (TeV) | 2.64 | | 3.74 | 6.48 |
| $\bar{q} + q\bar{q}$ | 2.631 | 10^0 | 5.064 | 10^0 |
| $q + q\bar{q}$ | 8.275 | 10^0 | 1.257 | 10^1 |
| $g + q\bar{q}$ | 1.522 | 10^1 | 3.248 | 10^1 |
| Total | 2.613 | 10^1 | 5.011 | 10^1 |
| | | | 1.276 | 10^2 |

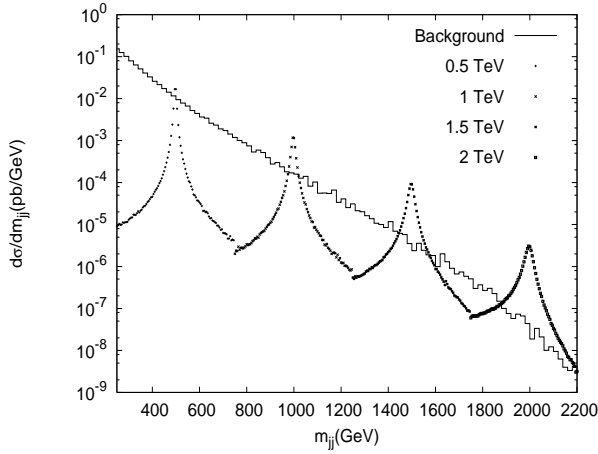


FIG . 7: The invariant mass distributions for the QCD background with the inclusion of scalar diquark signals at ep collisions.

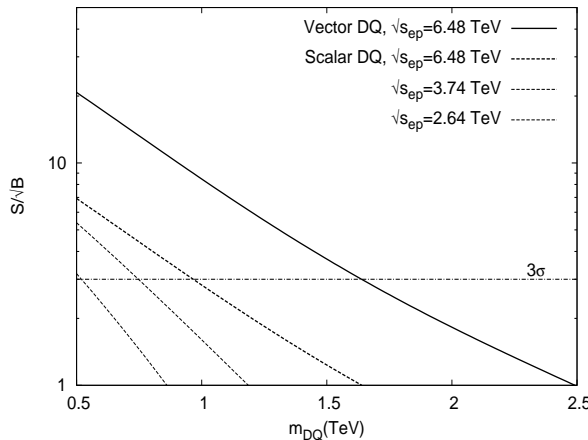


FIG . 8: The signal significances $S = \frac{\sigma}{B}$ as a function of scalar and vector diquark mass m_{DQ} at different ep collider energies.

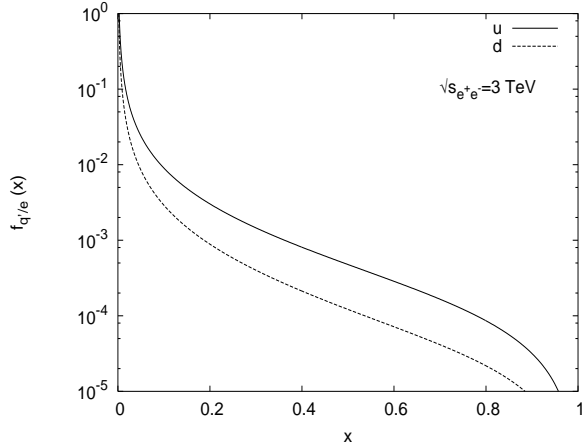


FIG. 9: The probability density for up (u) and down (d) quarks within electron beam for bremsstrahlung photons.

C. e^+e^- collider

The cross section for the production of a pair of jets through the two resolved photon process is given by

$$= \int_{x_{m \text{ in}}}^{x_{m \text{ max}}} dx \int_{y_{m \text{ in}}}^{y_{m \text{ max}}} dy f_{q=e}(x; Q^2) f_{q^0=e}(y; Q^2) b(b) \quad (15)$$

here $f_{q=e}(x; Q^2)$ and $f_{q^0=e}(y; Q^2)$ correspond to the probability density of finding a quark q and q^0 carrying a fraction x and y of the energy of the electrons and positrons in the initial beam s , respectively. In (15) the integrals over the momentum fractions x and y are the mathematical representation of an energy scan performed by the partons coming from electrons and positrons. The lower limits of the integrations guarantee the energy required for the production of quarks. As a consequence of this energy scan there will be quarks whose energies adequate for the resonance production of diquarks. For the probability $f_{q=e}(x; Q^2)$ resulting from the convolution of the spectrum of photons $f_{q=e}(x_2)$ converted from the initial beam s and photonic parton distribution function $f_{q=e}(x_1; Q^2)$ [17], we use

$$f_{q=e}(x; Q^2) = \int_{x_{2 \text{ min}}}^{x_{2 \text{ max}}} dx_2 \int_{x_{1 \text{ min}}}^{x_{1 \text{ max}}} dx_1 f_{q=e}(x_2) f_{q^0=e}(x_1; Q^2) (x_1 x_2 - x) \quad (16)$$

$$= \frac{1}{x_2} \int_x^{x_2} dx_2 f_{q^0=e}(x) f_{q^0=e}\left(\frac{x}{x_2}; Q^2\right) \quad (17)$$

For the relevant Q^2 value entering the parton distribution in the photon, we have taken $Q^2 = \frac{p_T^2}{b} = 2$:

In Fig. 9, the quark probability density $f_{q=e}(x; Q^2)$ within electron beam are presented for bremsstrahlung photons at beam energy $E_e = 1.5$ TeV.

Here, we show only u and d quark distributions in photon since we deal with only the first family diquarks. In Fig. 10 (a-b), the production cross section versus scalar and vector diquark mass is plotted for e^+e^- with the center of mass energy $\sqrt{s_{e^+e^-}} = 0.5; 1$ and 3 TeV:

The two-jet background receives contributions from the annihilation process $e^+e^- \rightarrow Z \rightarrow q\bar{q}$ and the hard two photon processes. The two photon processes can be of type direct, one resolved and two resolved. The last two processes, despite being higher order in s , contribute significantly at lower energies. The spectrum of initial state radiation (ISR, photon radiation from the incoming electrons and positrons) contains the ISR scale inherent to the process under consideration [19]. In our calculations, this spectrum is taken into account using the CompHEP program with the convolution of beam strahlung spectra. Beam strahlung is the process of energy loss by the incoming electron/positron in the field of the positron/electron bunch moving in the opposite direction. Beam strahlung spectrum is an attribute of the linear collider design and depends on the bunch geometry, bunch charge and the collision energy. The photon spectrum resulting from the electromagnetic interaction between the electron and positron beams in the intersection region is described by a more complicated expression [20]. The beam strahlung parameters, and

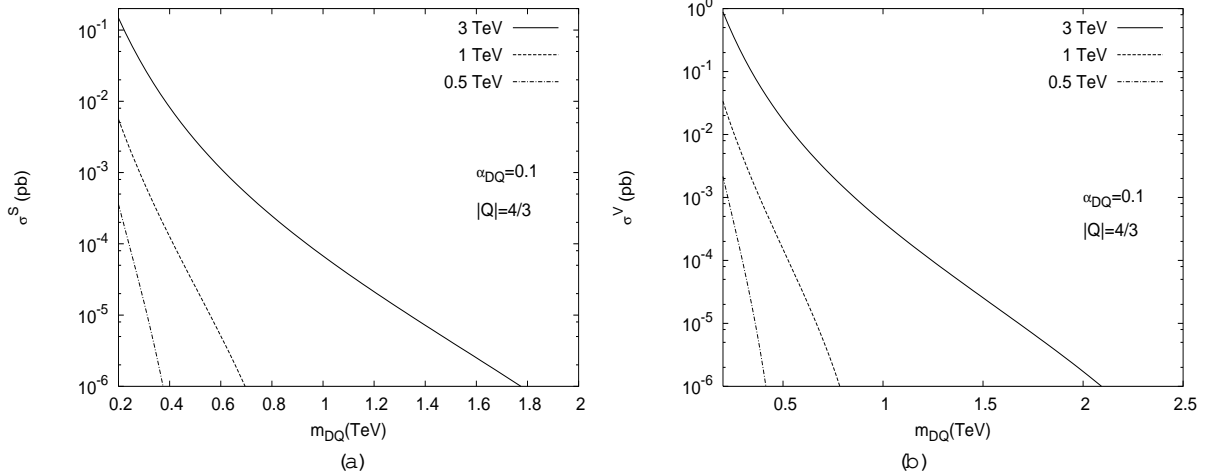


FIG. 10: The production cross sections for (a) scalar diquark and (b) vector diquark with charge $D = 4/3$ at e^+e^- colliders with $\frac{p_T}{S_{e^+e^-}} = 0.5; 1$ and 3 TeV, where the coupling $\alpha_{DQ} = 0.1$.

TABLE V : Collider parameters relevant for the calculation of beam strahlung. α is the beam strahlung parameter and N is the average number of photons per electron.

| Collider parameter | ILC | | | CLIC | | |
|--------------------|---------|-------|-------|---------|-------|-------|
| | 500 GeV | 1 TeV | 3 TeV | 500 GeV | 1 TeV | 3 TeV |
| $N (10^{10})$ | 2 | 0.4 | 0.4 | 2 | 0.4 | 0.4 |
| x (nm) | 655 | 115 | 43 | 655 | 115 | 43 |
| y (nm) | 5.7 | 1.75 | 1 | 5.7 | 1.75 | 1 |
| z (m) | 300 | 30 | 30 | 300 | 30 | 30 |
| α | 0.045 | 1.014 | 8.068 | 0.045 | 1.014 | 8.068 |
| N | 1.22 | 1.04 | 1.74 | 1.22 | 1.04 | 1.74 |

N , which in their turn are determined by the bunch design of a linear collider:

$$= \frac{5 N E_e}{6m_e^3 z (x + y)} ; \quad N = \frac{25^2 N}{12m_e (x + y)} \frac{1}{1 + \frac{p_T^2}{2z^2}} \quad (18)$$

where N is the number of particles in the bunch; E_e and m_e are the energy and mass of the electron, respectively; x , y and z are the average sizes of the particle bunches. We presented the beam strahlung parameters in Table V and their effects in the background calculations in Table VI.

We determine the expected significance of the signal over the background for collider parameters as given in Table I, for ILC operating at 500 GeV, CLIC operating at 1 and 3 TeV. For the realistic analysis of the background we consider the generic hadron calorimeters with the two-jet mass resolution $m_{jj} = 0.5 \frac{p_T}{m_{jj}} + 0.03 m_{jj}$. In order to reduce the background we vetoed events exhibiting Z -bosons decaying into two-jets through the cut $m_{jj} > 100$ GeV. In Fig. 11, we presented the contributions from both the annihilation process with/without ISR + beam strahlung and two-photon processes to dijet cross sections at $\frac{p_T}{S_{e^+e^-}} = 3$ TeV.

TABLE VI: Background calculation with the ISR and beam strahlung effects. The numbers are the cross sections in pb for the process $e^+e^- \rightarrow Z \rightarrow q\bar{q}$ with $p_T^j > 20$ GeV ($p_T^j > 100$ GeV).

| Collider parameter | ILC | | | CLIC | | |
|---------------------------|-------------|---------------|-----------------|-------------|---------------|-----------------|
| | 500 GeV | 1 TeV | 3 TeV | 500 GeV | 1 TeV | 3 TeV |
| no ISR | 2.22 (1.96) | 0.546 (0.672) | 0.0604 (0.0602) | 2.22 (1.96) | 0.546 (0.672) | 0.0604 (0.0602) |
| with ISR | 8.16 (2.11) | 1.96 (0.629) | 0.276 (0.0829) | 8.16 (2.11) | 1.96 (0.629) | 0.276 (0.0829) |
| with ISR + beam strahlung | 8.38 (2.16) | 4.30 (1.04) | 67.55 (1.39) | 8.38 (2.16) | 4.30 (1.04) | 67.55 (1.39) |

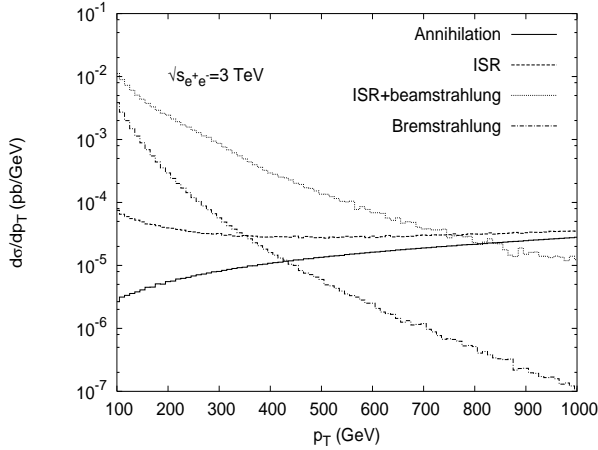


FIG . 11: The transverse momentum distributions of the jets.

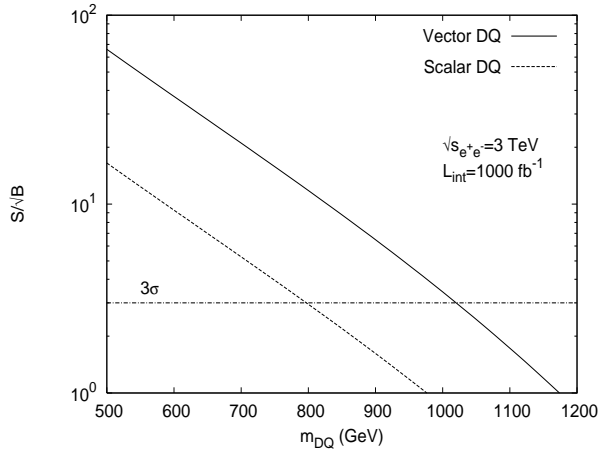


FIG . 12: The scalar and vector diquark signals significance as a function of their masses.

We conclude that signal significances scale with the collider luminosity as $\frac{p_T}{L}$; and higher luminosities are desirable for a good signal over background discrimination. In determining the background events we considered some cuts on transverse momentum $p_T > 100$ GeV of the jets. In Fig. 12, we present the signal significance that can be reached at e^+e^- collider with at $\frac{p_T}{\sqrt{s_{e^+e^-}}} = 3$ TeV.

We take the indication of signal $S = B = 3$ and find that vector diquarks can be probed up to 1 TeV at e^+e^- collider with $\frac{p_T}{\sqrt{s_{e^+e^-}}} = 3$ TeV. For the e^+e^- colliders running at the center of mass energy of 1 TeV we can search for scalar diquarks up to 325 GeV and vector diquarks up to 375 GeV.

V . CONCLUSION

The resonant production of scalar and vector diquarks at LHC have large cross section. With reasonable cuts, it may be possible to cover mass ranges up to 10 TeV for coupling $D = 0.1$. For smaller couplings as $D = 10^{-3}$, it is still possible to probe diquarks up to the mass of 4 TeV at an integrated luminosity $L = 10^2 \text{ fb}^{-1}$. We find that vector diquarks can be seen up to 1.6 TeV at the ep collider with $\frac{p_T}{\sqrt{s}} = 6.48$ TeV and a slightly lower limit can be obtained for scalar diquarks. The two hard photon processes prevail at energies below $\frac{p_T}{\sqrt{s}} = 2$ while the annihilation prevails at higher energies. Therefore, the attainable mass limits for diquarks are smaller than $\frac{p_T}{\sqrt{s}} = 2$ at linear colliders with the parameters given in Table I.

A limited number of measurements of diquark properties can be carried out at the hadron colliders. The future

high energy linear $e^+ e^-$ colliders and linac-ring type ep colliders based on the hadron and lepton colliders would complement the measurements performed at hadron colliders. The resolved photon contributions to the search for new physics becomes important for forthcoming ep and $e^+ e^-$ collisions.

Acknowledgments

This work is partially supported by the Turkish State Planning Organization (DPT) under the grant No 2002K 120250 and 2003K 120190.

- [1] J. Wudka, *Phys. Lett. B* 167 (1986) 337.
- [2] J. L. Hewett and T. G. Rizzo, *Phys. Rep.* 183 (1989) 193.
- [3] F. Abe et al., CDF Collaboration, *Phys. Rev. Lett.* 55 (1997) R 5263; T. Dorigo, FERMILAB-CONF-97-281-E, CDF-PUB-EXOTIC-PUBLIC-4238, (unpublished) (1997).
- [4] G. Bhattacharyya, D. Choudhury and K. Sridhar, *Phys. Lett. B* 355, (1995) 193.
- [5] A. G usso, *J. Phys. G: Nucl. Part. Phys.* 30, (2004) 691.
- [6] V. D. Angelopoulos et al., *Nucl. Phys. B* 292, (1987) 59.
- [7] E. N. Argyres, C. G. Papadopoulos, S. D. P. Vlassopoulos, *Phys. Lett. B* 202, (1988) 425.
- [8] S. Atag, O. Cakir, and S. Sultansoy, *Phys. Rev. D* 59, (1998) 015008.
- [9] E. Arrik, S. A. Cetin, O. Cakir, S. Sultansoy, *J. High Energy Phys. JHEP09* (2002) 024.
- [10] T. G. Rizzo, *Z. Phys. C* 43, (1989) 223.
- [11] P. Abreu et al., DELPHI Collaboration, *Phys. Lett. B* 446, 62 (1996).
- [12] Stefan Soldner-Rembold et al., OPAL Collaboration, 18th International Symposium On Lepton And Photon Interactions (LP 97) 28 Jul-1 Aug 1997, Hamburg, Germany; [hep-ex/9706003](#).
- [13] M. A. Doncheski and S. G. Odifrey, *Phys. Rev. D* 49, 6220 (1994); *ibid.* 51, 1040 (1995); *Phys. Lett. B* 393, 355 (1997); *Mod. Phys. Lett. A* 12, 1719 (1997).
- [14] H. L. Lai et al., CTEQ Collaboration, *Eur. Phys. J. C* 12, (2000) 375.
- [15] E. Boos et al., CompHEP Collaboration, CompHEP 4.4: Automatic computations from Lagrangians to events, *Nucl. Instrum. Meth. A* 534 (2004), p250, [hep-ph/0403113](#); CompHEP – a package for evaluation of Feynman diagrams and integration over multi-particle phase space. User's manual for version 3.3, [hep-ph/9908288](#).
- [16] ATLAS Collaboration, Detector and Physics Performance Technical Design Report, Volume 1, ATLAS TDR 14, CERN/LHCC 99-14, (1999) and Volume 2, ATLAS TDR 15, CERN/LHCC 99-15, (1999).
- [17] M. Glück, E. Reya, A. Vogt, *Phys. Rev. D* 46, (1992) 1973.
- [18] D. de Florian, S. Frixione, *Phys. Lett. B* 457, (1999) 236.
- [19] E. A. Kuraev and V. S. Fadin, *Sov. J. Nucl. Phys.* 41, 466 (1985).
- [20] P. Chen, *Phys. Rev. D* 46, 1186 (1992).